

Review of elastocaloric cooling systems and their performance

Yao Wang(王尧) and Suxin Qian(钱苏昕)

Citation: Chin. Phys. B, 2026, 35 (**7**): 077503. DOI: 10.1088/1674-1056/ae3692
http://cpb.iphy.ac.cn; http://iopscience.iop.org/cpb

What follows is a list of articles you may be interested in

Strain energy enhanced room-temperature magnetocaloric effect in Mn_5Ge_3

Xiaohe Liu(刘潇贺), Ping Song(宋平), Sen Yao(姚森), Yuhao Lei(雷雨豪), Ling Yang(杨玲), Shenxiang Du(杜深祥), Yiran Deng(邓贻然), and Defeng Guo(郭得峰)

Chin. Phys. B, 2026, 35 (**2**): 027505. DOI: 10.1088/1674-1056/adf6a6

Tuning the magnetocaloric and structural properties of $La_{0.67}Sr_{0.28}Pr_{0.05}Mn_{1-x}Co_xO_3$ refrigeration materials

Changji Xu(徐长吉), Xinyu Jiang(姜心雨), Zhengguang Zou(邹正光), Zhuojia Xie(谢卓家), Weijian Zhang(张伟建), and Min Feng(冯敏)

Chin. Phys. B, 2024, 33 (**12**): 127501. DOI: 10.1088/1674-1056/ad8550

Magnetic and magnetocaloric effect of $Er_{20}Ho_{20}Dy_{20}Cu_{20}Ni_{20}$ high-entropy metallic glass

Shi-Lin Yu(于世霖), Lu Tian(田路), Jun-Feng Wang(王俊峰), Xin-Guo Zhao(赵新国), Da Li(李达), Zhao-Jun Mo(莫兆军), and Bing Li(李昺)

Chin. Phys. B, 2024, 33 (**5**): 057502. DOI: 10.1088/1674-1056/ad1a94

Multicaloric and coupled-caloric effects

Jia-Zheng Hao(郝嘉政), Feng-Xia Hu(胡凤霞), Zi-Bing Yu(尉紫冰), Fei-Ran Shen(沈斐然), Hou-Bo Zhou(周厚博), Yi-Hong Gao(高怡红), Kai-Ming Qiao(乔凯明), Jia Li(李佳), Cheng Zhang(张丞), Wen-Hui Liang(梁文会), Jing Wang(王晶), Jun He(何峻), Ji-Rong Sun(孙继荣), Bao-Gen Shen(沈保根)

Chin. Phys. B, 2020, 29 (**4**): 047504. DOI: 10.1088/1674-1056/ab7da7

Effect of Sb-doping on martensitic transformation and magnetocaloric effect in Mn-rich $Mn_{50}Ni_{40}Sn_{10-x}Sb_x$ (x=1, 2, 3, and 4) alloys

Ishfaq Ahmad Shah, Najam ul Hassan, Jun Liu(刘俊), Yuanyuan Gong(龚元元), Guizhou Xu(徐桂舟), Feng Xu(徐锋)

Chin. Phys. B, 2017, 26 (**1**): 017501. DOI: 10.1088/1674-1056/26/1/017501

TOPICAL REVIEW — Multiferroicity and multicaloric effects

Review of elastocaloric cooling systems and their performance

Yao Wang(王尧)[1,2,†] and Suxin Qian(钱苏昕)[1,‡]

[1] *Department of Refrigeration and Cryogenic Engineering, School of Energy and Power Engineering, Xi'an Jiaotong University, Xi'an* 710049, *China*
[2] *Department of Mechanical and Aerospace Engineering, The Hong Kong University of Science and Technology, Kowloon, Hong Kong, China*

(Received 25 November 2025; revised manuscript received 6 January 2026; accepted manuscript online 12 January 2026)

Elastocaloric cooling offers a solid-state alternative to conventional vapor-compression systems by leveraging stress-induced phase transitions in materials like shape-memory alloys (SMAs). This review comprehensively analyzes the development and performance of elastocaloric cooling systems to date. We explain the thermodynamic mechanisms and material requirements, emphasizing challenges such as low latent heat and fatigue life. Subsequently, we categorize and compare thermal contact and heat-transfer-fluid (HTF)-based prototypes, discussing their achievements in temperature span and cooling power. The technical maturity of elastocaloric cooling systems is not comparable to that of commercial vapor-compression systems yet in terms of coefficient of performance (COP) and practicality. We further explore innovative approaches like work recovery, modular design, and novel loading modes (e.g., torsion) to bridge application gaps. The review concludes that elastocaloric cooling holds promise for sustainable refrigeration, though material fatigue, system COP, and heat transfer efficiency remain critical bottlenecks for future research.

Keywords: solid-state refrigeration, caloric cooling, elastocaloric cooling, shape-memory alloys, prototype development

PACS: 75.30.Sg, 65.40.G–, 44.27.+g, 44.10.+i

DOI: 10.1088/1674-1056/ae3692 **CSTR:** 32038.14.CPB.ae3692

1. Introduction

Cooling accounts for approximately 20% of global energy consumption and is recognized as one of the seven critical technologies to watch by 2025.[1,2] Notably, the World Economic Forum listed elastocaloric cooling among the Top 10 Emerging Technologies of 2024 to address global challenges.[3] This solid-state cooling exploits the latent heat induced by stress in materials such as shape-memory alloys (SMAs) and polymers. Specifically, applying mechanical stress drives a phase transformation from high-entropy austenite to low-entropy martensite, releasing latent heat and increasing temperature. Conversely, upon stress removal, the reverse transformation absorbs heat, leading to a temperature drop that enables cooling.[4] This mechanism embodies a direct and nominally reversible solid-state energy conversion between mechanical work and heat.

Elastocaloric cooling produces zero direct emissions, aligning with the demand for environmentally friendly development.[5] It is one of the so-called caloric cooling technologies, which utilize phase transitions driven by different external fields, including magnetocaloric,[6–8] electrocaloric,[9–13] and mechanocaloric.[14–16] Among these solid-state alternatives, elastocaloric cooling is particularly promising due to its large cooling power density and wide temperature span.[17] However, the performance of current elastocaloric cooling prototypes is constrained by limited material energy density and heat transfer efficiency, leading to a coefficient of performance (COP) that still trails that of traditional vapor-compression systems. This gap currently necessitates higher electrical energy input. Nevertheless, with the accelerating integration of clean energy sources[18] and advances in power generation such as controlled nuclear fusion,[19] future electricity grids are expected to become largely decarbonized. In this context, the inherent recyclability of elastocaloric materials[20] promises a truly sustainable, emission-free refrigeration solution over its full life cycle.

The realization of this potential is currently hampered by material limitations. Ideal elastocaloric materials should simultaneously exhibit large latent heat, low hysteresis, long fatigue life, high thermal conductivity, and low driving stress. However, existing materials, primarily SMAs, struggle to meet all these criteria concurrently. For instance, the gravimetric latent heat of typical elastocaloric materials rarely exceeds 35 $J\cdot g^{-1}$,[21] which is still lower than the 173.2 $J\cdot g^{-1}$ of the common vapor-compression refrigerant R134a,[22] despite the fact that their volumetric latent heat is similar. Furthermore, a trade-off often exists between latent heat and hysteresis; alloys achieving low hysteresis (e.g., Au–Cu–Zn[23]) typically exhibit modest latent heat.

Additionally, commercial materials like binary Ni–Ti

[†]Corresponding author. E-mail: refwangy@gmail.com
[‡]Corresponding author. E-mail: qiansuxin@xjtu.edu.cn

© 2026 Chinese Physical Society and IOP Publishing Ltd. All rights, including for text and data mining, AI training, and similar technologies, are reserved.

alloys require high driving stresses (400–600 MPa) to induce a relatively small transformation strain ($\sim 5\%$), necessitating actuators capable of "high force output with small displacement".[24] This requirement often leads to bulky and oversized actuators, increasing system mass and driving losses. Although new materials like Ni–Fe–Ga show potential for sub-100 MPa driving stresses,[25–27] they have not been implemented in any elastocaloric cooling system yet.

The concept of elastocaloric cooling technology was first proposed in 2002. After theoretical and experimental validation,[28] the first prototype was established in 2015.[29] This technology has evolved along two primary paths. The first focuses on thermal contact-based devices that leverage direct heat conduction between the solid refrigerants and heat sources/sinks.[30] To compensate for limited thermal conductivity, the elastocaloric materials in these systems are often fabricated into thin plates or fine wires, which inherently restricts the total refrigerant mass. Consequently, while contact-based prototypes can achieve appreciable temperature spans, their cooling power remains relatively low. Their key advantages lie in high reliability, low noise, and minimal vibration, making them suitable for specialized applications such as aerospace electronics cooling,[31] rather than for conventional domestic appliances. The second pathway incorporates heat transfer fluids (HTFs) into the system.[32]

Leveraging the good mechanical strength of elastocaloric materials, these materials can be engineered into efficient fluid-solid heat exchangers (regenerators).[33,34] Utilizing forced convection, these HTF-based prototypes have achieved a maximum temperature span of 75 K,[35] meeting the demands for applications like air conditioning and heat pumps.[36] Despite rapid progress toward commercial viability, challenges such as oversized actuators, low system COP, and high cost persist.

In this concise review, we elaborate on the fundamental mechanisms, material properties, and recent advancements in elastocaloric cooling systems. Section 2 discusses the thermodynamic mechanisms and material realization of elastocaloric effects. Section 3 reviews the development of thermal contact-based and HTF-based prototypes, introducing their key features and performance highlights. Section 4 examines the performance gaps towards practical applications and discusses innovative solutions aimed at overcoming these challenges. Finally, we conclude with an outlook on the future development of this promising technology.

2. Elastocaloric materials

2.1. Phase transition

Elastocaloric materials form the cornerstone of elastocaloric cooling technology, with SMAs and shape memory polymers (e.g., natural rubber) being the primary candidates. While polymers can achieve an adiabatic temperature change of approximately 10 K under a low driving stress (< 50 MPa), their limited fatigue life and low thermal conductivity have impeded progress in this area.[37–39] Consequently, the mainstream development of elastocaloric cooling remains centered on SMAs, particularly commercial binary Ni–Ti and Ni–Ti-based alloys.

A cooling device operates on the principle of the second law of thermodynamics, expending energy to pump heat from a low-temperature source to a high-temperature sink. Continuous refrigeration is achieved by implementing a thermodynamic cycle. As depicted in Figs. 1(a) and 1(b), the basic cycle for elastocaloric materials comprises four fundamental steps. (1) Loading process: external stress induces a phase transformation (e.g., austenite to martensite in Ni–Ti alloys), releasing latent heat and causing a temperature rise. (2) Exothermic process: while stress/strain is maintained, heat is rejected to a heat sink, returning the material to its initial temperature. (3) Unloading process: removal of the external stress allows the material to revert to its initial phase, absorbing latent heat and resulting in a temperature drop. (4) Endothermic process: the cooled material absorbs heat from the heat source, thereby providing the cooling effect. These four processes utilize the reversible phase transition of the elastocaloric material to transfer energy from the cold side to the hot side. The fundamental cost of this cycle is the driving work required during the loading process. The relaxation time of the material's deformation ($\sim 10^{-2}$ s) is significantly shorter than the characteristic time constant of heat transfer ($> 10^{-1}$ s).[40] This temporal disparity necessitates the separation of the loading/unloading process from the exothermic/endothermic process within the cycle.

The elastocaloric effect originates from a first-order reversible phase transition. The latent heat, fundamental to this effect, stems from the entropy difference between phases, such as martensite and austenite in SMAs. This relationship is quantitatively described by the Clausius–Clapeyron equation[41]

$$\left(\frac{\mathrm{d}\sigma}{\mathrm{d}T}\right)_{\mathrm{SMA}} = -\frac{\rho \Delta s}{\varepsilon_{\mathrm{M}}}. \tag{1}$$

This equation characterizes the temperature dependence of the phase transformation stress, defining the constitutive behaviour of the martensitic transformation. Here, ρ is the material density ($\mathrm{kg\cdot m^{-3}}$), Δs is the entropy change ($\mathrm{J\cdot kg^{-1}\cdot K^{-1}}$), and ε_{M} is the transformation strain. To maximize the cooling capacity per cycle, elastocaloric materials must exhibit a large entropy change, corresponding to a high latent heat.

Constitutive modelling of elastocaloric materials generally follows two approaches: one establishes phenomenolog-

ical relationships based on microstructural features or experimental data;[42–45] the other derives the intrinsic material behaviour from a thermodynamic perspective by formulating a free energy function and incorporating dissipation potentials consistent with the second law of thermodynamics. Models adhering to thermodynamic principles are often interrelated despite differing methodologies. The free energy curves for different phases in a SMA can be schematically represented as in Fig. 1(c), where $\Delta G^{\mathrm{A-M}}$ denotes the Gibbs free energy barrier for martensite nucleation, and represents the approximate thermodynamic equilibrium temperature, $T_{\mathrm{p0}} = (T_{\mathrm{Ms}} + T_{\mathrm{As}})/2$. The total Gibbs free energy change during phase transition is given by

$$\Delta G = \Delta G_{\mathrm{c}} + \Delta G_{\mathrm{s}} + \Delta G_{\mathrm{e}} = \Delta G_{\mathrm{c}} + \Delta G_{\mathrm{nc}}. \tag{2}$$

Here, ΔG_{c} represents the chemical energy change during the phase transition, ΔG_{s} denotes the interfacial free energy, ΔG_{e} corresponds to the elastic energy term, and ΔG_{nc} is the sum of non-chemical energy terms. SMAs require an undercooling or superheating temperature to facilitate the nucleation of martensite or austenite within the material. When the driving force applied to the material is sufficiently large, the influence of the stress field on SMAs becomes the dominant factor. In such cases, the entropy change during the phase transition can be described by Eq. (1). During the reversible phase transition of elastocaloric materials, irreversible entropy generation occurs due to intergranular friction in the phase transition process of shape memory alloys. This entropy generation is influenced by factors such as material composition, fatigue life, and operating conditions. The irreversibility of the phase transition is also reflected in the characteristic of phase transformation hysteresis: at the same temperature, the stress required for austenite transformation is higher than that for martensite transformation. A larger phase transformation hysteresis corresponds to greater irreversible losses and a shorter fatigue life of the material.[46] Therefore, ideal elastocaloric refrigerants should possess as low a phase transformation hysteresis as possible, along with a high latent heat of phase transition.

The thermodynamic behavior of SMAs in elastocaloric cooling devices can be described by models such as the Müller–Achenbach–Seelecke model.[47–49] Consistent with Eq. (2), the key energy contributions are the chemical potential and the non-chemical (elastic) potential. The potential energies of the martensite and austenite phases can be expressed by Eqs. (3) and (4), respectively. In these equations, the first term on the right-hand side represents the elastic potential, while the second term, β, denotes the chemical potential. Here, M^{+} and M^{-} refer to the phase fractions transformed under tensile and compressive stresses, respectively.

$$\Phi_{\mathrm{M}\pm}(\varepsilon, T) = \frac{E_{\mathrm{M}}}{2}(\varepsilon \mp \varepsilon_T)^2 + \beta_{\mathrm{M}}(T), \tag{3}$$

$$\Phi_{\mathrm{A}}(\varepsilon, T) = \frac{E_{\mathrm{A}}}{2}\varepsilon^2 + \beta_{\mathrm{A}}(T). \tag{4}$$

The phase evolution in an elastocaloric cycle can be delineated into six sequential stages: elastic loading of austenite, stress-induced austenite-to-martensite transformation, fully martensitic state, elastic unloading of martensite, reverse martensite-to-austenite transformation, and final unloading of austenite. The work due to volumetric changes is represented by the stress-strain term, leading to the relationship between Gibbs free energy (G) and Helmholtz free energy (Ψ). Analyzing these six stages allows the derivation of the transformation stress–temperature correlations, as shown below:[50,51]

$$G(\sigma, \varepsilon, T) = \Psi(T) - \sigma\varepsilon, \tag{5}$$

$$\sigma_{\mathrm{AM}}(T) = E_{\mathrm{A}}(T)\gamma_{\mathrm{A}}(T), \tag{6}$$

$$\sigma_{\mathrm{MA}}(T) = E_{\mathrm{M}}(T)(\gamma_{\mathrm{A}}(T) - \varepsilon_T). \tag{7}$$

Here, E and γ represent the nodal values at different stages of the cycle, specifically, the elastic modulus and strain nodes at unstable states as detailed in Ref. [52].

Alternatively, a linearized form describing the transformation stress versus temperature can be obtained directly from the Clausius–Clapeyron relation (Eq. (1))

$$\sigma_{\alpha\beta}(T) = \sigma^0_{\alpha\beta}(T) + C^0_{\alpha\beta}(T - T_{\mathrm{ref}}), \tag{8}$$

where α and β denote the austenite and martensite phases, respectively. The first term on the right-hand side represents the transformation stress at the reference temperature T_{ref}. The coefficient $C_{\alpha\beta}$ is the reciprocal value derived from Eq. (1).

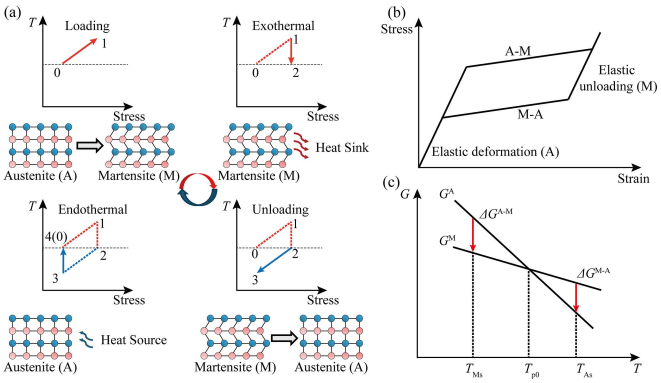


Fig. 1. Material state variation during the elastocaloric cooling cycle. (a) Variations in temperature, stress, and phase composition of the material (refer to Ref. [53]). (b) The stress–strain curves of the material during elastocaloric cooling cycle. (c) Gibbs free energy curves of austenite–martensite phases in elastocaloric materials (refer to Ref. [41]).

2.2. Materials performance

The practical application of elastocaloric cooling in industrial systems imposes stringent requirements on material properties. Ideal elastocaloric materials must simultaneously exhibit large latent heat, low hysteresis, high yield stress, good ductility, long fatigue life, and low cost.[36] Furthermore, since these materials are engineered into heat exchangers (regenerators) to enable efficient heat transfer, low phase transition

stress and high thermal conductivity are also critical for enhancing the stability and overall performance of the heat exchange unit.

A large latent heat of phase transition is the fundamental requirement for achieving substantial cooling capacity. Although latent heat values vary among different SMAs, they generally struggle to exceed 35 $J \cdot g^{-1}$. Moreover, some large latent-heat materials require very high stress at near-room temperature.[21] Figure 2(a) presents the latent heat and martensitic/austenitic transformation temperatures of several typical shape memory alloys. The latent heat originates from the difference in Gibbs free energy between the parent phases and the product transition. Once the primary elements of an alloy are determined, its fundamental electronic structure and chemical bonding characteristics become relatively fixed. Consequently, compositional adjustments typically yield only a continuous, smooth variation in latent heat rather than a discontinuous jump, with limited impact on the total energy of the system. Therefore, achieving a breakthrough in the latent heat of existing materials is exceedingly challenging without the discovery of entirely new material systems.

Besides latent heat, fatigue life is the most critical factor for practical applications. Household refrigeration systems operate for up to 4380 hours annually.[54] Assuming a typical operating frequency of 1 Hz for an elastocaloric cooling device, the annual cycle count would exceed 15 million. Fortunately, advanced SMAs can achieve stable operation for over 10 million cycles,[55–57] as shown in Fig. 2(b). System-level strategies, such as parallel design with multiple units operating collectively, can reduce the duty cycle of individual components, thereby extending the overall system service life. In summary, while the fatigue performance of existing materials is adequate for the prototype stage, further improvements at both the material and device design levels are essential for long-term continuous operation.

Another challenge at the device level is the oversized actuator. The high phase transition stress of elastocaloric materials (e.g., for Ni–Ti, $>$ 800 MPa in compression and $>$ 500 MPa in tension, as shown in Fig. 2(c)), and their small strain ($\sim$ 5%) necessitate actuators capable of delivering high force with small displacement. This driving requirement is contrary to that of commercial motors. Therefore, in current prototypes, oversized drivers need to be configured to meet the driving force requirement. Although the actual driving power (the product of driving force and deformation) required by the material is not large, its significant driving force requirement causes significant driving losses in the system. Table 1 shows the mass proportion of actuators in several typical prototypes. The excessively high driving force currently needed is one of the major constraints on the development of elastocaloric cooling prototypes.

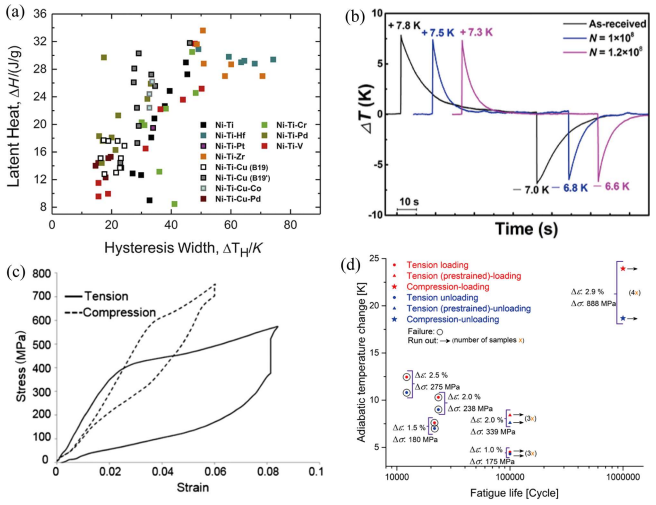


Fig. 2. Performance of elastocaloric materials. (a) Hysteresis width versus latent heat of the typical Ni–Ti-based materials.[61] (b) Temperature profiles of the high fatigue-life Ni–Ti at different numbers of cycles.[55] (c) Stress–strain curve comparison between tension and compression for polycrystalline Ni–Ti within the austenite state.[58] (d) Adiabatic temperature changes of Ni–Ti alloy as functions of fatigue-life under tension and compression at different applied strains/stresses.[62]

Table 1. Performance and drive device/solid refrigerant mass ratio of typical prototypes.

Prototype	Specific cooling power ($W \cdot g^{-1}$)	Temperature span (°C)	Drive device/solid refrigerant mass ratio	References
HTF-based single-stage compressive Ni–Ti tubes with HTF	0.48	4.7	1: 750	[63,64]
Thermal contact-based single-stage Ni–Ti foils	7.7	13	1: 960	[30,65]
Regenerative tensile stacked Ni–Ti plates	0.78	19.9	1: 2,800	[66,67]
Tensile Ni–Ti wire assembly	0.34	9.8	1: 389	[68]
Tensile two-stage Ti–Ni–Cu plate with work recovery	0.38	25.4	1: 193	[69]
Compressive Ni–Ti tubes	31.6	12.3	1: 479	[70]

Furthermore, the loading method has a decisive impact on system performance, fatigue, and the actuator simultaneously. Compressive stress-driven methods exhibit superior fatigue performance compared to tensile-driven ones, as stress concentration induced by microcracks in tension can significantly reduce fatigue life.[58] However, when the target temperature difference is below 25 K (household refrigeration) and with strict strain limitations ($\leq$2%) to ensure tensile fatigue life, tensile-driven parallel-plate structures demonstrate higher energy efficiency and cooling power. This is attributed to their excellent heat transfer performance. At a 15 K temperature difference, their cooling capacity and COP can reach

values that are 3.5 and 2.8 times those of compression designs, respectively, making them the superior choice in such scenarios.[59] Therefore, the loading method for a practical device depends on its application scenarios and performance demands. Consequently, elastocaloric materials with lower phase transition stresses are highly desirable for practical applications. For instance, alloys such as Ni–Fe–Ga can achieve complete phase transformation under stresses below 100 MPa. Although their latent heat is relatively low (~ 5 J·g^{-1}), the reduced stress enables the integration of a larger mass of refrigerant within the same system, potentially enhancing the overall cooling capacity. Furthermore, polymer materials like rubber also exhibit the elastocaloric effect, requiring significantly lower driving stresses and demonstrating considerable potential.[60]

Hysteresis represents the intrinsic irreversible energy loss during the phase transition, which directly reduces the material's effective cooling power and narrows the achievable temperature span. The cooling cycle converts mechanical energy to thermal energy via the elastocaloric material. The ideal maximum thermal energy is the full latent heat, while the ideal minimum mechanical energy is the hysteresis work. The original material COP is defined by Eq. (9). Thus, low-hysteresis materials can enhance the energy efficiency of elastocaloric cooling systems.[71] This original definition describes the cost and the output of the elastocaloric material, but it ignores the inherent heat transfer temperature difference in the cooling cycle. This zero temperature span between the heat source and the heat sink cannot be used to evaluate second-law efficiency. Therefore, adopting the Stirling cycle, which contains the isothermal loading/unloading and two isostrain regeneration processes, a temperature-dependent material COP can be defined by Eq. (10).[72] This definition of material COP provides an evaluation at different operating temperatures and can be used to derive the second-law efficiency.

$$\mathrm{COP}_{\mathrm{mat}} = \frac{\rho c_{\mathrm{p}} \Delta T_{\mathrm{ad}}}{\oint \sigma \,\mathrm{d}\varepsilon}, \tag{9}$$

$$\mathrm{COP}_{\mathrm{mat,Stirling}} = \frac{T_{\mathrm{c}}(\Delta s - s_{\mathrm{gen}})}{(T_{\mathrm{h}} - T_{\mathrm{c}})\Delta s + (T_{\mathrm{h}} + T_{\mathrm{c}})\, s_{\mathrm{gen}}}, \tag{10}$$

where ΔT_{ad} is adiabatic temperature change (°C). T_{c} and T_{h} are the temperatures of the heat source and the heat sink, respectively (°C). s is the specific entropy (J·g^{-1}·K^{-1}). s_{gen} is the entropy generation (J·g^{-1}·K^{-1}).

Beyond intrinsic material properties, advanced processing and manufacturing techniques offer pathways to overcome current bottlenecks. For instance, creating a graded transformation temperature distribution through specific heat treatments[73] enables more uniform heat exchange with the HTF, reducing heat loss and improving efficiency.[35] Additive manufacturing demonstrates significant potential for addressing limitations in temperature span, cooling power, and cyclic stability.[74] The design of functionally graded and porous structures provided by additive manufacturing presents novel avenues for higher efficiency. Theoretical analyses indicate that porous structures can achieve a specific cooling power 3.55 times higher than parallel-plate regenerators, with a theoretical maximum exceeding 80 W·g^{-1}.[75] Finally, as recyclable solid-state materials, elastocaloric materials can regain their cooling performance through processes such as remelting and regeneration. By remelting Ni–Ti scrap with calcium and halide fluxes,[20] elastocaloric materials hold the potential to achieve efficient recycling.

2.3. Criteria for elastocaloric materials

The fundamental performance metrics for elastocaloric materials are well-defined, emphasizing large latent heat, long fatigue life, and small hysteresis. To achieve better performance, the material properties required for different elastocaloric cooling systems may vary. For tension-driven systems, the material is subjected directly to tensile stress, making it sensitive to defects and requiring high toughness and uniformity. Such systems require only relatively low stress to trigger the phase transformation. In contrast, compression-driven systems must prevent buckling failure, demanding materials with high stiffness and structural support against buckling. These systems often enhance stability through bundled tubes or additional support structures, thereby reducing the material's inherent requirement for bending resistance. Higher stress is needed in compression, which can be addressed by optimizing the material through microtextured design and similar methods.

From the heat transfer perspective, for thermal-contact-based systems, a smooth surface finish is usually preferred since it features less thermal contact resistance. However, for fluid-based systems, a rough surface is better for inducing turbulence and promoting heat transfer performance. For tube-shaped materials applied in elastocaloric regenerators, if the materials are segmented such that the fluid flows in the transverse direction,[76–78] higher thermal conductivity is preferred. On the other hand, if the fluid flows in the axial direction of tube-shaped regenerators,[67,79] anisotropic thermal conductivity is ideal, with high thermal conductivity in the transverse direction and low thermal conductivity in the axial (loading) direction. In the case of isotropic thermal conductivity, a moderate value is favored to minimize diffusion loss.

From an application perspective, three key considerations determine the common requirements of an elastocaloric material: the ability to meet performance requirements in a compact form factor, the capability for continuous and stable operation, and overall cost-effectiveness. First, regarding performance and compactness, elastocaloric devices must satisfy the fundamental performance criteria for refrigeration and

heat pump units, as detailed in Table 2. Given that the latent heat of current elastocaloric material systems is unlikely to increase by an order of magnitude in the short term, achieving a compact design with high cooling power remains challenging. Consequently, near-term applications are primarily anticipated in near-room-temperature household appliances, such as refrigerators and air conditioners. To enhance device compactness, materials with lower phase-transformation stresses, such as Cu–Zn–Al and Ni–Fe–Ga alloys, are promising candidates. The elastocaloric properties of shape memory alloys vary with composition and microstructure. For example, Cu-based alloys (Cu–Zn–Al) can achieve an entropy change of approximately 20 $J{\cdot}kg^{-1}{\cdot}K^{-1}$ under low stress ($\sim$ 100 MPa), but exhibit a relatively low adiabatic temperature change ($\sim$ 10 K). In contrast, Ni–Ti alloys require higher stress ($\sim$ 500 MPa).[80] Although the latent heat of such materials is typically lower than that of high-stress variants like Ti–Ni, the ratio of latent heat to applied stress provides a valuable metric for comparing the cooling potential of different material systems, indicating the amount of latent heat a material can deliver per unit mechanical force input. Furthermore, as heat exchange inherently involves a temperature difference, a portion of the material's maximum temperature drop (ΔT_{d}) cannot be utilized for cooling. Therefore, the parameter $\rho c_{\mathrm{p}}(\Delta T_{\mathrm{d}} - \Delta T_{\mathrm{HT}})/\sigma\varepsilon$ (where ΔT_{HT} is the heat-transfer temperature difference, assumed to be 5 °C) is employed to evaluate different material systems. For instance, using this metric, $Ni_{50.8}Ti_{49.2}$ and $Ni_{54}Fe_{19}Ga_{27}$ are 11.2 and 15.7, respectively.[26] Although the driving stress of Ni–Fe–Ga at room temperature (250 MPa) is significantly lower than the driving force required for Ni–Ti (600 MPa), when comprehensively considering the influence of latent heat and heat exchange capacity, Ni–Ti remains the material capable of enabling a more compact system architecture.

Table 2. The cooling power and system temperature span requirements of typical refrigeration units*.

		Cooling power (W)	System temperature span** (°C)
Household appliances	air conditioner	> 800	25
	refrigerator	> 80	20
Commercial appliances	refrigerated cabinets	> 200	25
	variable refrigerant flow system	> 5000	20
Industrial appliances	cold store	> 10000	20
Advanced elastocaloric cooling prototypes		1260	75

*Data from the following Chinese standards: GB/T 7725-2022, GB/T 8059-2016, GB/T 21001.2-2015, GB/T 21454-2021, and GB 50072-2021.
**Assuming 5 K heat transfer temperature difference on each side.

Second, the continuous and stable operation of an elastocaloric device is fundamentally governed by the material's fatigue life. As outlined in Subsection 2.2, an elastocaloric air conditioner would require the material to withstand approximately 15 million cycles annually, assuming 4380 hours of operation and a 1 Hz operating frequency. According to the Chinese standard GB/T 46738, which stipulates a safe service life of 10 years for air conditioners, the material must endure about 150 million cycles over its lifetime. For a household refrigerator, referencing the durability requirements for mechanical components (e.g., doors and drawers) in the Chinese standard GB/T 8059 and assuming a typical lifespan of 13 years with 10 door cycles per day, the requisite number of cycles is determined by the cooling system's operation. If the system operates 12 hours daily at 1 Hz, the material in an elastocaloric refrigerator would need to withstand approximately 205 million cycles over 13 years. Crucially, as standard material fatigue testing often excludes real-world operational factors, the experimentally measured fatigue performance tends to be higher than the achievable service life in commercial products.

Therefore, without additional system-level requirements for material replacement, a paramount requirement for the commercialization of elastocaloric technology is the material's ability to retain sufficient elastocaloric performance over more than 200 million cycles.

Finally, concerning cost, elastocaloric devices will likely remain at a disadvantage in the short term, though this challenge is not insurmountable. Currently, these elastocaloric devices exist primarily as laboratory prototypes at the exploratory stage, with core components such as materials, frames, and actuators often custom-made, leading to high costs. However, should elastocaloric technology advance to assembly-line production and incorporate efficient material recycling strategies as previously discussed, the cost structure would shift significantly. The focus would then be primarily on electricity consumption during operation and initial manufacturing expenses, resulting in a substantial overall cost reduction. Given that research on the recycling and reuse of elastocaloric materials remains an area with significant gaps, it represents a promising and critical direction for future development in the field of elastocaloric materials. Moreover, if the efficient regeneration technology of materials can achieve a breakthrough, allowing us to directly regenerate the elastocaloric materials in the device, then the demand for fatigue life of elastocaloric materials will be greatly reduced.

3. Elastocaloric cooling prototypes

The pioneering work of Qian *et al.*[63] in 2015 marked the first demonstration of the HTF-based elastocaloric cooling prototype. This prototype utilized tubular NiTi to achieve a maximum adiabatic temperature change of 4.7 K and a cooling capacity of 65 W. Bruederlin *et al.*[30] developed a thermal contact-based prototype employing 0.03 mm thin-film Ni–Ti–Fe, generating a temperature span of approximately 13 °C at 3 Hz. These early prototypes established two distinct development pathways for elastocaloric cooling technology: one relying on direct contact heat exchange, and the other utilizing convective heat transfer with the HTF. The former approach reduces heat exchange complexity and offers inherent device compactness. However, constrained by the limited heat flux of thermal conduction and its strong dependence on contact area, such systems typically struggle to achieve high cooling power. In contrast, HTF-based systems can deliver significantly greater cooling power but incur increased complexity from additional fluid networks and inherent thermal losses associated with the intermediate heat transfer medium. These two system types have since evolved with distinct characteristics and application targets.

3.1. Thermal contact-based elastocaloric cooling prototypes

Thermal contact-based elastocaloric cooling devices utilize solid-state heat conduction, emphasizing the solid characteristics of the refrigerant.[81] While this approach benefits from compactness, low vibration, and high reliability, the inherently lower efficiency of thermal conduction compared to forced convection limits the achievable cooling power. To mitigate the prolonged heat exchange times, elastocaloric materials in these systems are typically fabricated into thin plates or fine wires. This design constraint naturally steers such all-solid-state devices toward miniaturized applications. Their advantages make them particularly suitable for specialized fields where reliability and compactness outweigh the need for high cooling power, such as in aerospace thermal management.[31] Furthermore, the solid-state nature of this technology also makes it promising for low-temperature refrigeration.[82] Demonstrations include Ni–Ti–Co alloys generating a temperature change of 3.68 K at −150 °C[83] and Cu–Al–Mn alloys exhibiting the elastocaloric effect around 4.2 K,[84] indicating potential for cryogenic all-solid-state coolers. However, the development of cryogenic elastocaloric coolers faces two primary challenges. First, the adiabatic temperature change (ΔT_{ad}) diminishes at lower temperatures due to its proportionality to the absolute temperature ($T\Delta s/c_p$), complicating heat exchange at cryogenic levels. Second, the high stress required to induce martensitic transformation at cryogenic temperatures risks causing irreversible plastic deformation, leading to functional fatigue. Currently, research on room-temperature thermal contact-based prototypes has validated the influence of various design factors, including actuation methods, cascaded (multi-stage) configurations, and work recovery systems, alongside preliminary attempts at product development.

A typical prototype employs an electric motor to drive reciprocating motion, alternately bringing the SMA foil into contact with the heat sink and heat source.[85] Cascading multiple stages is an effective strategy to amplify the temperature span for such devices. For instance, a three-stage system increased the temperature span from 7.6 K to 15 K.[86] An optimized design, illustrated in Fig. 3, using three cascaded Ni–Ti–Fe films achieved a notable temperature span of 27 K with a specific cooling power of 3.4 $W\cdot g^{-1}$.[87] Further performance gains are possible by increasing the operating frequency and refining materials. Using ultra-thin Ni–Ti–Cu–Co (0.08 mm) enabled a specific cooling power of 18 $W\cdot g^{-1}$.[88] In addition, system performance can also be enhanced by increasing the refrigerant mass and implementing innovative operational strategies, such as work recovery mechanisms using cams or linkages. Moreover, to address the challenge of high driving forces, Sharar *et al.*[89,90] implemented a bending actuation method, achieving a significantly improved actuator-to-refrigerant mass ratio of 9.7:1, where 20.7 g of elastocaloric material obtained a temperature change of 6 °C. However, the bending actuation method results in only the bent section of the material undergoing sufficient deformation, leading to a relatively low utilization efficiency of the refrigerant material.

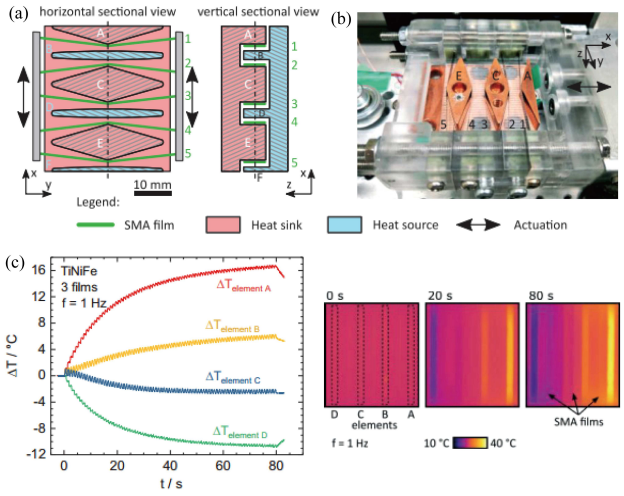


Fig. 3. SMA film-based elastocaloric cooling prototype.[87] (a) Schematic setup of the parallelized elastocaloric cooling device. (b) The experimental device with the five SMA films, the frame, and the heat sink. The heat source is not included to enable the view of the SMA film. (c) Temperature evolution of the copper elements of the cascaded elastocaloric cooling device at 1 Hz. (d) Infrared thermographs of the cooling device during operation in the experiment.

Many early prototypes focused on performance bench-

marking using copper blocks as heat sources, with less emphasis on practical integration. However, Chen *et al.* made significant strides toward commercialization by developing a compact refrigerator using a single-motor guided rail mechanism, as shown in Fig. 4(a).[68] This device, employing a 9-g bundle of Ni–Ti wires (outer diameter: 0.7 mm), cooled a 0.9 L insulated chamber, achieving a temperature difference of 9.2 °C and a cooling power of 3.1 W. This performance surpasses that of a comparable commercial thermoelectric cooler (1.1 W), highlighting the market potential of this technology. A subsequent advancement, illustrated in Fig. 4(b) by Yao *et al.*, combined material and system innovation.[69] They used a Ti–Ni–Cu alloy with a nanocrystalline structure for lower hysteresis and integrated it into a two-stage, roller-driven cooler with a novel kinetic energy recovery system (78% efficiency). This synergy yielded a dramatic performance improvement, achieving a maximum temperature span of 25.4 K and a cooling power of 6.7 W.

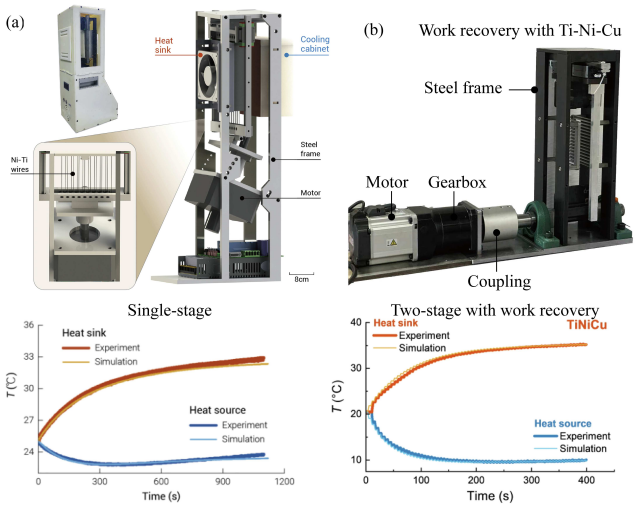


Fig. 4. (a) The compact thermal contact-based elastocaloric refrigerator, and the experimental and simulated temperature changing trends of the heat sink and heat source.[68] (b) Photo of the prototype of the refrigerator with work recovery, and the temperature changing trends within Ti–Ni-Cu (refer to Ref. [69]).

A fundamental challenge for thermal contact-based devices arises from the heat transfer mechanism itself. Relying on solid conduction necessitates that the elastocaloric material maintains sufficient, unobstructed surface area for heat exchange. This requirement often precludes the use of full peripheral support structures, making the material less suitable for robust compression-driven configurations, which generally offer better fatigue life. This limitation poses a significant challenge to the durability and practical application of tensile-driven devices. A promising solution to this interfacial challenge was introduced by Zhang *et al.*, who incorporated non-reciprocal heat transfer units into an all-solid-state system.[91] This innovative design switches the heat flow direction via internal rotation while maintaining constant physical contact between the elastocaloric material and the heat source/sink, and eliminates the periodic making and breaking of contacts, thereby avoiding the associated issues of increasing interfacial thermal resistance and degradation of contact force. It enables more stable and efficient heat transfer, achieving a temperature span of 4.3 K under no-load conditions and opening a new pathway toward high-performance, fluid-free cooling. Other thermal control concepts, such as thermal diodes, thermal regulators, and thermal switches, could possibly be integrated into such solid-state devices.[92,93]

In summary, thermal contact-based elastocaloric devices, which operate by cyclically deforming the material and bringing it into contact with heat sources and sinks, offer key advantages of simplicity, compactness, and reliability. However, they are generally characterized by relatively low system-level performance, fatigue life concerns under tensile loading, and inefficient material utilization in bending modes. Therefore, this technology is currently more suited for miniaturized devices and specialized applications where compactness, low noise, and high reliability are prioritized over large cooling capacity. For instance, miniaturized electronic devices generate substantial heat flux during high-performance operation, resulting in the formation of local hotspots and temperature fluctuations. These thermal management challenges can induce wavelength shifts, power instability, and reliability degradation in optical components, such as lasers and modulators.[94] Advanced solid-state cooling methods, such as micro-thermoelectric coolers, demonstrate considerable application potential in such scenarios.[95] Elastocaloric cooling, which concurrently embodies the advantages of solid-state cooling (e.g., quiet operation, high reliability) and exhibits high cooling capacity, warrants further exploration for thermal management of miniaturized chips and integrated circuits. It is envisioned as a complementary technology rather than a direct replacement for mainstream vapor-compression systems in the foreseeable future.

3.2. HTF-based elastocaloric cooling prototypes

HTF-based elastocaloric cooling systems effectively utilize the latent heat of the refrigerant via convective heat transfer, enabling performance that meets the requirements for near-room-temperature refrigeration applications. The core component of such devices is the elastocaloric regenerator, which is a fluid–solid heat exchanger designed to maximize heat transfer performance while maintaining structural integrity under cyclic loading. A primary strategy for enhancing regenerator performance is to increase its specific heat transfer area (heat transfer area per unit mass of elastocaloric material) through innovative structural design. Additional approaches include implementing a graded distribution of phase transition temperatures along the regenerator to optimize heat exchange efficiency. The push toward commercialization has

also spurred the exploration of modular devices and heat-driven systems. Based on the material architecture and loading method, regenerators can be broadly classified into three categories: (1) stacked-plate assemblies, (2) compressed tubular structures, and (3) bending-driven wires or plates.

The stacked-plate configuration represents one of the earliest regenerator designs. As illustrated in Fig. 5(a), a regenerator composed of nine stacked Ni–Ti plates, with fluid channels formed between them, achieved a temperature span of 15.3 K in a heat pump application.[67] This design offers simplicity and a high specific surface area. However, its reliance on tensile stress driving can compromise fatigue life. Furthermore, the need for additional containment structures to form fluid channels raises challenges related to sealing and long-term mechanical stability. Although a significant milestone, this design is now less common in cutting-edge research. An alternative stacked-plate concept with potential for practical application is the perforated-plate stack, as patented by Exergyn Limited[96] and shown in Fig. 5(e). This design stacks perforated Ni–Ti plates to create numerous parallel fluid channels and is driven by compressive stress. The thin individual plates (0.75–1.25 mm) resist yielding, offering a promising new direction for practical applications,[97] though public performance data remain limited and require further validation.

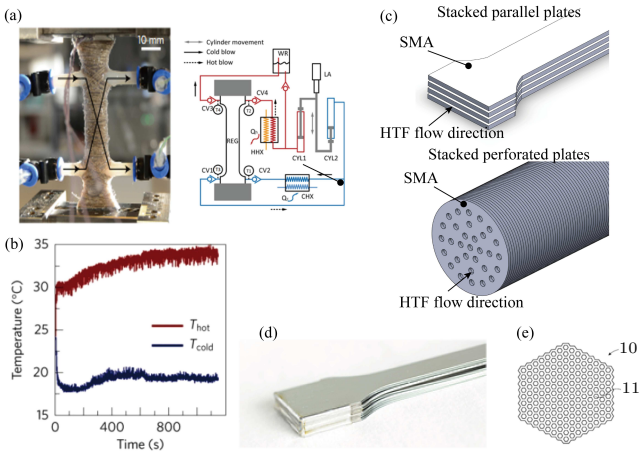


Fig. 5. (a) A photo of the stacked plate regenerator and the experimental setup.[66,67] (b) The temperature span between the heat sink and the heat source. (c) Schematic configuration of stacked parallel plates and perforated plates. (d) Photo of the plate regenerator. (e) A plan view of a hexagonal-shaped SMA structure.[96]

In contrast to plate-based structures, tubular elastocaloric materials are inherently suitable for constructing compressively stressed regenerators and represent the current forefront of prototype development. These tubular regenerators are categorized by the HTF flow path: internal flow through the tubes or external flow over tube bundles. The first elastocaloric cooling prototype employed internal flow within smooth Ni–Ti tubes, achieving a cooling power of 65 W.[63] Building on this, Qian *et al.* used a bundle of 19 Ni–Ti tubes to demonstrate two fundamental operating modes (Fig. 6).[79] The first operating mode employs an active regenerative cycle to establish the maximum temperature gradient within the regenerator, achieving a maximum temperature change of 22.5 °C. In this mode, the latent heat of the material enables the HTF to develop a temperature gradient along the regenerator, resulting in the maximum temperature span between the regenerator's inlet and outlet. The second operating mode allows the HTF to fully exchange heat within the regenerator before proceeding to the heat source/sink, converting all the latent heat into cooling power, thereby achieving a maximum cooling capacity of 260 W.

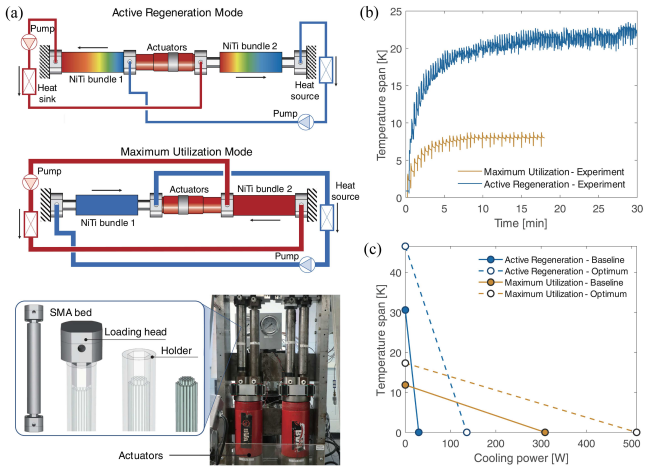


Fig. 6. (a) System design schematics and the operating principles of the elastocaloric cooling system. The active regeneration mode is used for achieving a large temperature span. The maximum utilization mode provides enhanced cooling power. (b) The performance of the multimode elastocaloric prototype: the evolution of temperature span as a function of time. (c) Temperature span versus cooling power of the prototype.[79]

To enhance performance, subsequent research focused on increasing the heat transfer area. Zhang *et al.*[98] introduced internal grooving in Ni–Ti tubes (Fig. 7(a)), which extended the fatigue life beyond 2 million cycles and increased specific cooling power and temperature span by 53% and 33%, respectively. Following this design, Zhou *et al.*[99] fabricated Ni–Ti tubes with an internal Archimedean spiral structure using wire-cut electrical discharge machining (Fig. 7(b)). Despite a challenging aspect ratio (50 mm length, 0.3 mm wall thickness) that exceeds typical buckling limits for compressed Ni–Ti,[100] the tubes enclosed by supporters showed stable performance over 1 million cycles and an impressive adiabatic temperature change of 50.6 K. This group later transitioned to a multi-cell Ni–Ti tube structure (Fig. 7(d)), creating a regenerator with graded phase transition temperatures that achieved a record temperature span of 75 K.[35] With further optimizations like nanofluids and series-parallel flow, a cooling power of 1260 W was reported at zero temperature span; the practical cooling power at a $\sim$ 8 K span of cooled air is estimated to be $\sim$ 100 W based on data in Fig. 7(e).[70]

External flow configurations, where the HTF passes over bundles of tubes or compressed assemblies, have also been

actively investigated.[101] Studies by Ahcin *et al.*[102] and Emaikwu *et al.*[76] confirmed that such refrigerators maintain high efficiency over many cycles. Ianniciello *et al.* developed a durable miniaturized system using eight Ni–Ti tubes with polylactic acid (PLA) flow distributors, which optimized heat transfer and minimized tube bending, operating for over 10^6 cycles with a 5 K temperature difference.[77] Ahcin *et al.* achieved a 31.3 K temperature span by segmenting a long Ni–Ti tube into a multi-stage system (Fig. 8), delivering 48.7 W of cooling at a 10.7 K temperature span.[78]

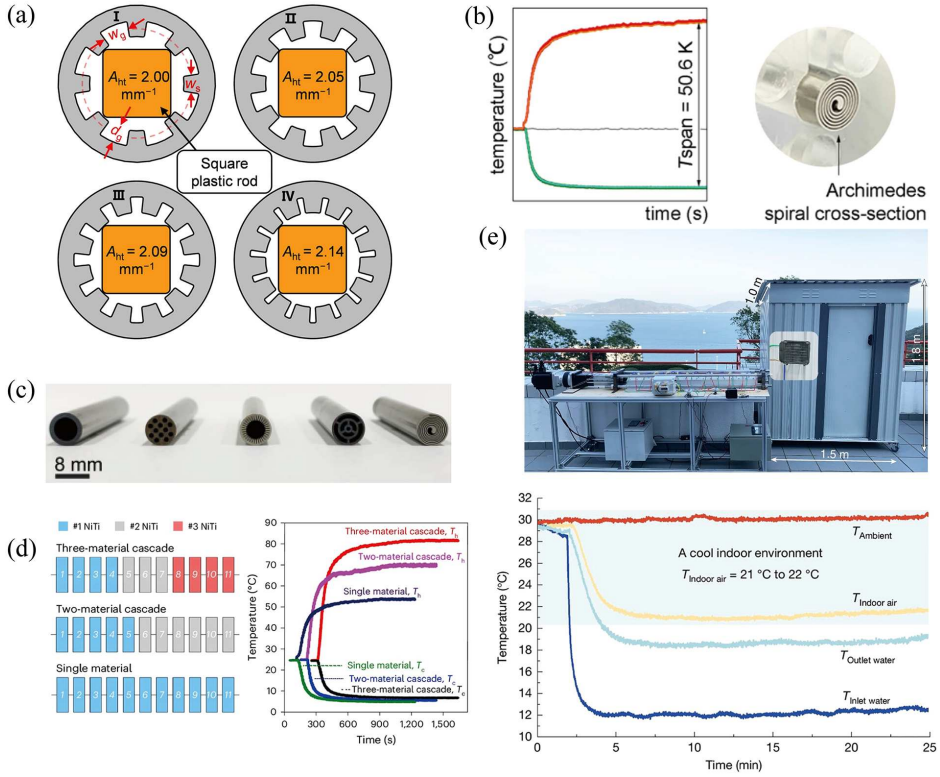


Fig. 7. (a) Cross-section of the longitudinally grooved Ni–Ti tubes.[98] (b) The photo of Archimedes spiral tube and the envelope of the temperature span between the heat sink and the heat source.[100] (c) Different customized shapes and geometries of SMA tubes. (d) The architecture of the cascaded materials and the evolution of temperature.[35] (e) An air-conditioning unit to cool a 2.7 m^{-3} model house based on the kilowatt-scale elastocaloric cooling. Indoor air temperature reached around 21–22 °C within 15 min (outdoor temperature of about 30–31 °C).[70]

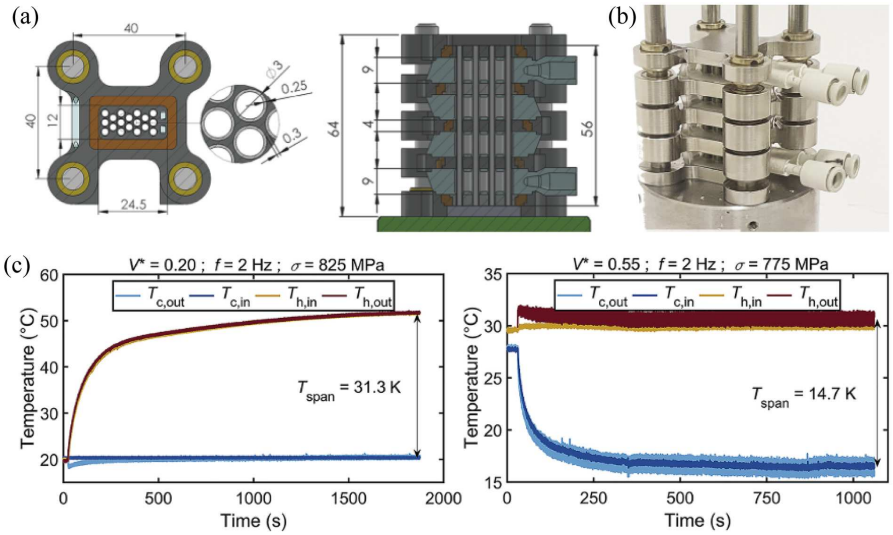


Fig. 8. The elastocaloric cooling prototype based on the external flow configurations.[78] (a) Schematics of the regenerator. (b) The photo of the regenerator. (c) The evolution of the temperature span in heat-pumping mode (left) and the cooling mode (right).

The distinctions between external flow and internal flow configurations lie in the permissible length of individual tubes and the design of the filler/support structures. For external flow around tubes, additional support structures cannot be placed outside the Ni–Ti tubes, as this would impede heat transfer between the HTF and the elastocaloric material. Since the material inevitably deforms during operation, any external support structure would need features like slots or gaps

to relieve radial forces exerted by the material. Conversely, internal support structures, which require tight contact with the elastocaloric materials to provide sufficient and stable support, introduce pre-stress. This pre-stress can paradoxically increase the risk of material failure. Therefore, internal flow designs can adopt supports, allowing the use of tubes longer than 30 mm within the system. In contrast, external flow designs are typically limited to tubes shorter than 15 mm (e.g., outer diameter ~ 3 mm, wall thickness ~ 1 mm).[100] Consequently, increasing the mass of elastocaloric materials in internal flow systems is achieved by increasing both the number and length of tubes, whereas external flow systems rely primarily on increasing the tube count.[103] This fundamental difference dictates their respective design optimization strategies: internal flow systems often employ axial grading of phase transition temperature along the tube length (to ensure uniform heat exchange temperature differences under large fluid temperature gradients), while external flow systems focus on fluid path design and optimized tube bundle distribution.

While uniaxial tension/compression enables complete phase transformation, it requires bulky actuators, and cyclic phase transitions can initiate cracks, limiting the fatigue life of commercial materials to 10^5 cycles.[89] Bending actuation presents a compelling alternative, requiring a force 6.09–7.75 times smaller and exhibiting 1.40–4.07 times lower hysteresis work per unit mass than tension for the same strain (e.g., 6%), enabling smaller, lighter, and more efficient actuators.

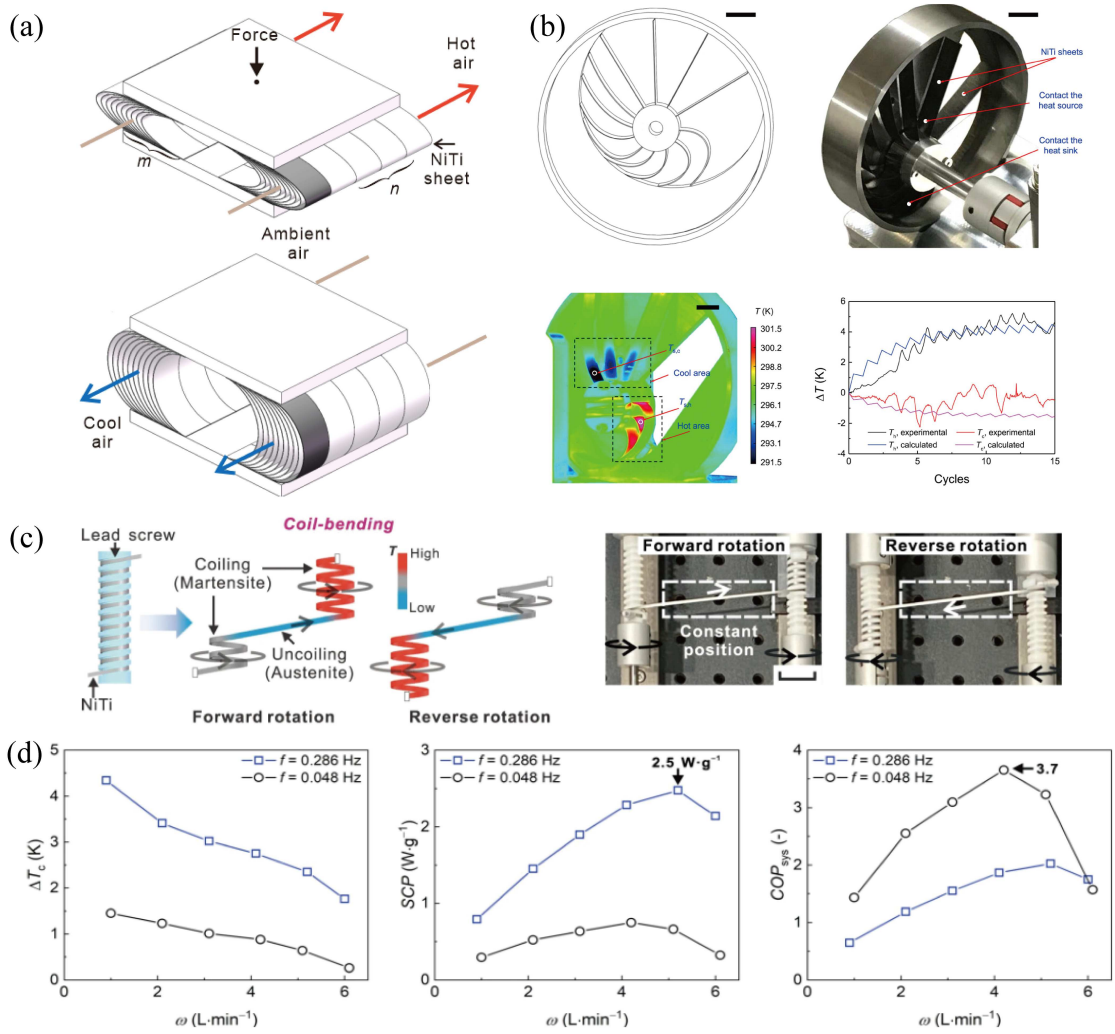


Fig. 9. Typical bending-based elastocaloric prototypes. (a) The compact elastocaloric air cooler based on bending Ni–Ti sheets.[104] (b) Schematic of continuous rotating bending Ni–Ti sheets.[105] (c) The coil-bending elastocaloric air cooler. (d) Cooling performances of the coil-bending air cooler.[106]

A compact elastocaloric air cooler based on bending Ni–Ti was introduced in 2022.[104] Its core mechanism, shown in Fig. 9(a), uses a two-point bending principle driven by a low-force actuator, reducing the specific driving force to 5.64 $\mathrm{N\cdot g^{-1}}$. It achieved a 5.5 K air temperature drop. A key innovation was using air directly as the HTF, avoiding liquid sealing, though this limits the specific cooling power (0.137 $\mathrm{W\cdot g^{-1}}$). Limitations included intermittent operation and non-uniform strain. Subsequently, Cheng *et al*. introduced a rotating bent-cantilever structure for continuous operation, as presented in Fig. 9(b).[105] This design features multiple Ni–Ti plates fixed to a rotating shaft, periodically contacting

copper heat sinks and sources to physically separate hot and cold zones. Model analysis revealed a temperature gradient along the length of the Ni–Ti sheets, with a maximum tensile strain of 6.2%. Heat flux increased with higher air flow rates. Experiments confirmed a stable temperature difference of 8–9 K at rotational speeds of 1.2–12 rpm. Emulating a loom's shuttle mechanism, Li *et al*. proposed a coil-bending structure for Ni–Ti wires, illustrated in Fig. 9(c), further reducing the specific driving force to 26 $N \cdot g^{-1}$ and achieving a specific heat transfer area of 12.6 $cm^2 \cdot g^{-1}$.[106,107] This design achieved an air temperature drop of 10.6 K, a specific cooling power of 2.5 $W \cdot g^{-1}$, and a system COP of 3.7, showcasing high efficiency in a compact volume ($300 \times 250 \times 200$ mm^3). In these bending-based devices, where air serves as both the HTF and the cooling target, the combination of low driving stress and minimized heat exchange stages results in the highest energy efficiency ratios among current HTF-based elastocaloric cooling systems.

Consequently, HTF-based and thermal-contact-based elastocaloric systems possess distinct advantages and disadvantages. The key advantages of thermal-contact-based systems are their compactness, high reliability, and low vibration, making them ideal for specialized miniaturized applications. However, they are fundamentally limited by their scalability, resulting in relatively lower cooling power than HTF-based systems. Furthermore, achieving good fatigue life is challenging, especially under tensile loading. In contrast, HTF-based systems have demonstrated record-breaking temperature spans up to 75 K and cooling powers exceeding 1 kW. The trade-off for this higher performance is increased system complexity from fluid networks, larger actuators required for high forces, and associated thermal losses. Therefore, while thermal-contact-based systems excel in compactness and reliability for niche applications, HTF-based systems are superior in cooling performance and are closer to practical viability for large-scale cooling, such as air conditioners.

4. Application challenges and innovative solutions

Elastocaloric cooling technology has predominantly utilized Ni–Ti-based alloys, establishing the mainstream developmental pathway. State-of-the-art prototypes have achieved notable performance benchmarks, including a cooling power exceeding 1 kW and a temperature span of over 75 K. Nevertheless, significant gaps persist when compared with conventional cooling systems operating near ambient temperature. These disparities are multifaceted:

(1) Performance evaluation metrics The cooling power of elastocaloric cooling prototypes is frequently reported without corresponding temperature span data, deviating from standard industry practices for evaluating traditional systems like air conditioning. For instance, most studies only reported cooling power at zero temperature span. In contrast, residential air conditioners typically require over 2000 W of cooling capacity at temperature drops exceeding 20 K.[108] Adopting established evaluation standards (see Table 3) is crucial for meaningful performance comparisons and assessing practical viability.

Table 3. Rating conditions for commercial refrigeration products and performance requirements for practical elastocaloric cooling systems.[36]

Category	T_c (°C)	T_h (°C)	Cooling (heating) power and corresponding ΔT_{span}[a]	ΔT_{span} at 0 load (K)[b]
Split-type air-conditioner (cooling)	15.5[c]	35	25 kW at 29.5 K	59
Split-type air-conditioner (heat pump)	–7	20	3.0 kW at 37 K	74
Domestic refrigerator (fresh food)	4	32	100 W at 38 K	76
Dehumidifier	23.7[d]	27	1 kW at 13.3 K	26.6

[a]Assuming 5 K heat transfer temperature difference on each side.
[b]Assuming a linear characteristic curve between the temperature span and cooling/heating power, which implies that the maximum cooling/heating power is twice the value listed in the table.
[c]Dew point temperature corresponding to the standard dry bulb of 27 °C and wet bulb of 19 °C.
[d]Dew point temperature corresponding to the standard dry bulb of 27 °C and wet bulb of 24 °C.

(2) System mass and volume The size and mass of elastocaloric systems are often dominated by the actuator, which must deliver high forces due to the substantial phase transition stresses required by current materials. Although bending-based actuation reduces force requirements, challenges such as limited fatigue life and inefficient material utilization continue to hinder commercial application. The cost, size, and weight of the final system are critical determinants of commercial competitiveness.

(3) Energy efficiency While the theoretical COP of elastocaloric materials can be high, the maximum system-level COP demonstrated by prototypes capable of delivering useful cooling is currently 1.3.[69] This is substantially lower than that of commercial air conditioning systems, which must meet stringent standards such as China's grade I energy efficiency requirement of COP > 5.8.[109] While the measured COP of current prototypes shows a significant gap compared to conventional systems, numerical simulation studies reveal substantial potential for optimization. By systematically optimizing the heat transfer process, for instance, using parameters like the heat utilization ratio to guide the design, the COP of Ni–Ti and Cu–Al–Zn systems can theoretically be increased

to 13.7 and 9.2, respectively.[110]

(4) Sustainability and recyclability The use of solid refrigerants eliminates direct emissions and supports a circular life cycle through material recycling. Coupled with an increasingly decarbonized electricity supply, elastocaloric cooling technology aligns with the United Nations' sustainable development goals for refrigeration.[111] However, comprehensive strategies for the full regeneration and recycling of elastocaloric materials and components remain an area requiring further research.

Addressing these practical challenges necessitates the concurrent development of application-specific solutions that leverage the intrinsic advantages of elastocaloric cooling. Currently, the primary development directions for elastocaloric refrigeration technology continue to align with the content outlined in Section 3. In brief, the mainstream efforts can be categorized as follows: (a) pursuing material performance optimization to incorporate more active material within devices; (b) optimizing existing material structures to achieve higher specific heat transfer area or improved fluid channel design; and (c) enhancing system performance through strategies such as integrating work recovery systems. These directions contribute to steady and effective improvements in the system's cooling capacity. However, given the significant performance gap compared to traditional vapor-compression refrigeration, this paper argues that application-oriented elastocaloric cooling research must introduce unique and novel concepts. Beyond serving as a replacement for conventional technology, elastocaloric cooling should also aim to fill application niches that existing technologies cannot address. Consequently, the remainder of this section introduces innovative design concepts that have the potential for rapid application or that address gaps left by current technologies.

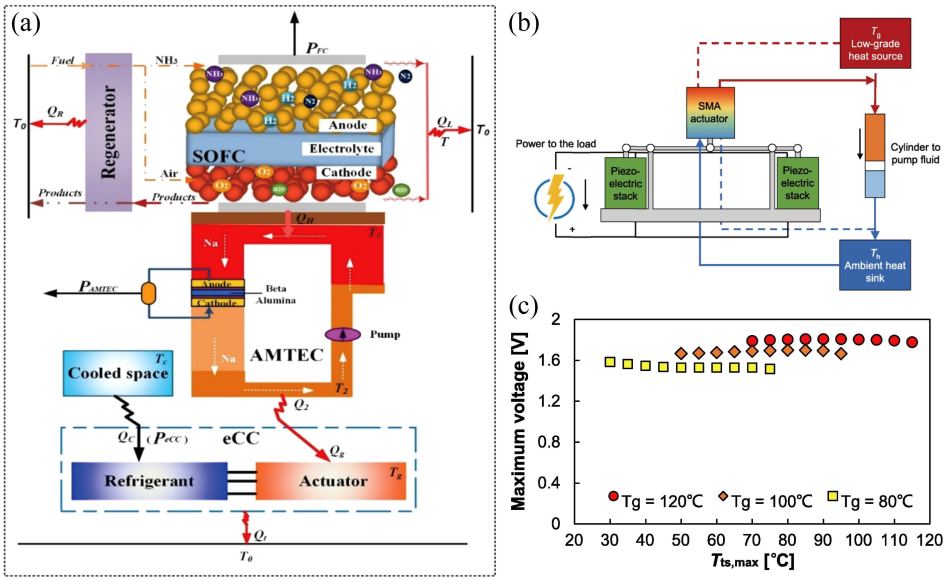


Fig. 10. Heat-driven and elastocaloric functional module coupling system. (a) Schematics of a triple-cycle system.[116] (b) Schematic of coupled elastocaloric actuator and piezoelectric generator.[119] (c) Performance of the elastocaloric-piezoelectric coupled system.

(1) Heat-driven and elastocaloric functional module coupling system The reversibility of the thermo-mechanical conversion in elastocaloric materials enables innovative heat-driven strategies. Coupling an SMA actuator with an elastocaloric cooling unit provides the heat-driven elastocaloric cooling method.[112] This approach significantly reduces the volume and mass of prototypes and facilitates the development of fully modular refrigeration devices. By implementing a transition temperature gradient[113] or a double-effect cycle,[114] such systems enable cascade utilization of input heat, boosting the COP above 0.8 and operating effectively with low-grade heat sources at 80–150 °C, thus offering an efficient solution for waste heat recovery. Following this method, the heat-driven elastocaloric actuator can absorb heat from other functional modules, such as fuel cells[115,116] and photovoltaic cells.[117,118] Figure 10(a) demonstrates a triple-cycle system.[116] The NH_3-solid oxide fuel cell (SOFC) module generates electricity and waste heat through an electrochemical reaction. The waste heat is first utilized by an alkali metal thermal electric converter (AMTEC) for thermal-to-electric conversion. The remaining thermal energy is then used by a heat-driven elastocaloric cooling system to provide cooling. Since a temperature-induced elastocaloric actuator can operate near room temperature, such module coupling systems realize the hierarchical utilization of energy. Moreover, alternative drive technologies capable of delivering "high force with small displacement" can also be explored for elastocaloric cooling. For example, coupling piezoelectric materials with elastocaloric materials theoretically demonstrated the feasibility for thermal-to-electrical energy conversion in Fig. 10(b).[119] This indicates that piezoelectric actuators can be a potential driving module for elastocaloric cool-

ing thanks to their driving characteristics of high driving force and small displacement.[120] Consequently, these functional module coupling systems can solve the problem of excessive volume during the application of elastocaloric prototypes, and also represent a novel attempt at system energy recovery and efficient utilization.

(2) Modular design for serviceability The quantifiable mechanical output and solid-state nature of elastocaloric materials facilitate modular design, where the refrigerant itself can serve as a replaceable structural component. This approach promises easier maintenance and extended system life. Ehl *et al*. demonstrated this concept, illustrated in Fig. 11(a), with a prototype using pre-fabricated, pre-trained Ni–Ti bundles that can be rapidly replaced.[121] This "mini-fridge" successfully cooled a chamber containing a 0.25 L beverage can by $\sim$ 3.5 K. This modular design concept indicates that elastocaloric devices can easily replace materials, which is important for practical applications. On one hand, this can make the recovery of the material more convenient; on the other hand, because the elastocaloric material itself occupies a relatively small space in the system, this design may solve the fatigue problem of the material during long-term operation by storing spare elastocaloric materials.

(3) Phase-change heat transfer Enhancing performance requires moving beyond material development to system-level innovation. Integrating phase-change heat transfer, which offers orders-of-magnitude higher heat transfer coefficients compared to single-phase convection, is a promising avenue. Bachmann *et al.* proposed an active elastocaloric heat pipe in Fig. 11(b), where the compression-induced temperature change of the solid refrigerant drives an evaporation-condensation cycle in a working fluid of water.[122,123] While the initial prototype achieved a modest maximum temperature span of 5.6 K and a cooling power of 7.9 W at 1.2 Hz, it successfully demonstrated the feasibility of harnessing phase-change heat transfer in elastocaloric systems.

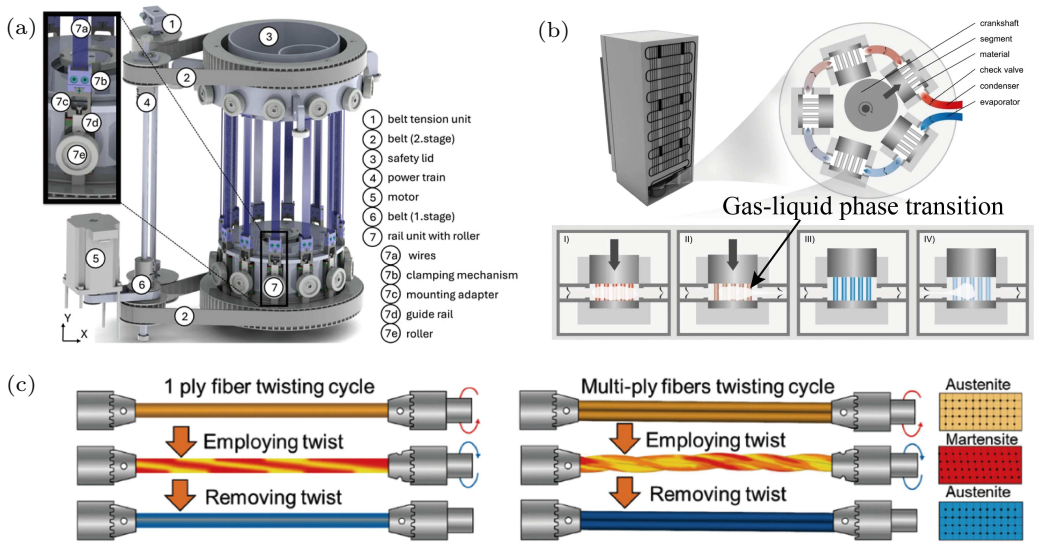


Fig. 11. (a) The elastocaloric can cooler uses prefabricated, pretrained Ni–Ti bundles that can be rapidly replaced.[121] (b) Schematic of an active elastocaloric heat pipe adopting HTF phase-change heat transfer.[122] (c) Schematic illustration of the elastocaloric cycle for Ni–Ti wires subjected to twisting and untwisting.[125]

(4) Alternative driving modes The driving methods discussed above primarily include uniaxial tension, compression, and bending of elastocaloric materials to trigger phase transformation. Nevertheless, other driving methods beyond these three conventional methods present potential avenues for application. By inducing reversible phase transformation through torsional stress, efficient elastocaloric cooling can be achieved with a low driving force.[124] In the Ni–Ti alloy system, a single torsional cycle can produce a cooling temperature drop of up to 18 K, while a series-connected twistocaloric heat pump can further increase the average temperature span to 25.6 K.[125] The maximum specific cooling power achieved by twistocaloric devices is 1.85 $W{\cdot}g^{-1}$, with a device cooling power of 5.0 W, which is competitive in compact cooling systems. When using HTF, the device based on three Ni–Ti wires operating at a cycling frequency of 0.2 Hz can achieve a sustained cooling fluid temperature difference of 7.7 K. The critical torsional stress is low (approximately 252 MPa), and the required torque is only 0.0834 N·m, equivalent to the force needed to manually open a bottle cap, far lower than the compression/tensile force required for elastocaloric cooling (10–15 kN).[126] Benefiting from torsion inhibiting crack propagation and dislocation accumulation, the fatigue life of twisted NiTi alloys is significantly improved, from about 1000 cycles for uniaxial tension to 14752 cycles,[125] and can even exceed 10000 cycles through gradient structure design.[127]

(5) Polymer-based elastocaloric materials Polymers, particularly natural rubber, have garnered significant attention due to their low cost, biodegradability, and exceptional elastocaloric properties. Adiabatic temperature

changes of up to 23 K have been achieved in natural rubber through strain-induced crystallization and optimized material formulations, such as uniform molecular chain lengths.[128] The incorporation of nanofillers like graphene nanoplatelets boosts the isothermal entropy changes, reaching 1.87 $J{\cdot}g^{-1}{\cdot}K^{-1}$.[129] Advanced polymer-based elastocaloric devices, including dual-unit regenerators,[130] snap-through instability mechanisms,[131] and bistable actuation systems,[132] have enabled high specific cooling powers up to 20.9 $W{\cdot}g^{-1}$[131] and a COP ranging from 4 to 16 under near-room-temperature operations.[130,133] These designs facilitate efficient heat transfer through solid–solid or solid–fluid interactions, with some systems achieving temperature spans of 7–9 K[130,131] in single-stage setups and work recovery efficiencies of up to 56.3%.[132] Despite these achievements, the low thermal conductivity of polymers (0.14 $W{\cdot}m^{-1}{\cdot}K^{-1}$ for natural rubber) leads to significant thermal losses and limits heat exchange rates. Experimental devices typically achieve only 40%–60% of the material's adiabatic temperature span.[134] Fatigue life under cyclic loading remains a concern, with natural rubber exhibiting degradation after 104–107 cycles depending on pre-strain levels.[131] Additionally, while COP values can reach $\sim$ 16, they often drop at higher frequencies or larger temperature spans due to parasitic heat flows. Future efforts for practical devices should focus on improving heat exchange efficiency, enhancing thermal conductivity, and modifying fatigue resistance.

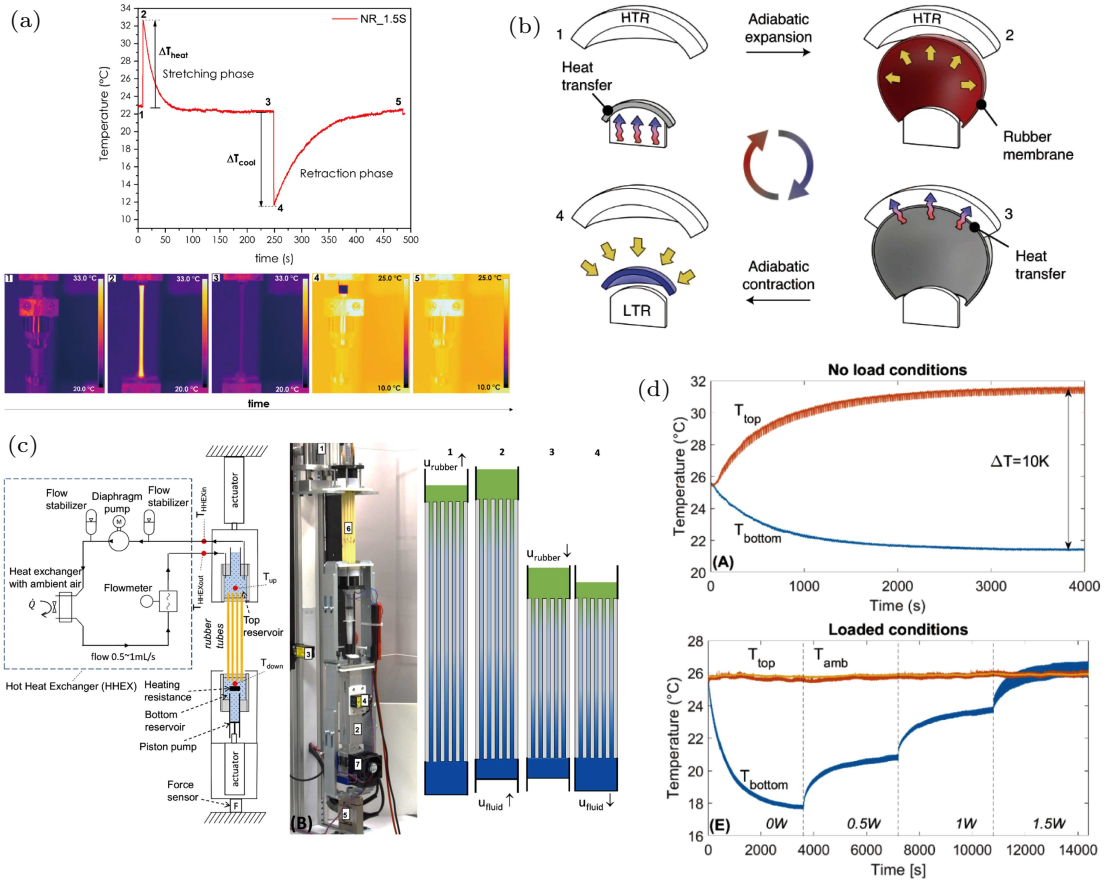


Fig. 12. Polymer-based elastocaloric cooling. (a) Performance of natural rubber.[134] (b) Principle of the elastocaloric heat pump based on natural rubber.[131] (c) Photo and experimental setup of the polymer-based regenerative elastocaloric cooler.[39] (d) The regenerative elastocaloric cooler performances under both unloaded and loaded conditions.

5. Conclusion and outlook

Elastocaloric cooling has emerged as a promising solid-state alternative to conventional vapor-compression refrigeration. Significant progress has been made in both thermal contact-based systems, which offer advantages in compactness and reliability for specialized applications, and HTF-based systems, which demonstrate superior cooling power and temperature spans approaching practical requirements. However, despite achieving remarkable benchmarks — including temperature spans exceeding 75 K and cooling powers over 1000 W in laboratory settings — current elastocaloric prototypes still face substantial gaps in energy efficiency (with COP rarely exceeding 1.3), system compactness, and long-term durability compared to commercial refrigeration systems.

The primary challenges lie in material limitations and system-level integration. The gravimetric latent heat of existing SMAs remains lower than that of traditional refrigerants, while high driving stresses necessitate bulky actuators, result-

ing in unfavourable device-to-refrigerant mass ratios. Furthermore, material fatigue life and heat transfer efficiency continue to constrain practical implementation. Nevertheless, innovative approaches are emerging to address these bottlenecks. These include the development of low-stress alloys and polymer-based composites, advanced manufacturing techniques for optimized regenerator structures, and novel system concepts such as heat-driven cycles, torsional loading modes, and modular designs that enhance serviceability and functional integration.

The future development of elastocaloric cooling should focus on several strategic directions. First, material innovation remains paramount, with research needed on high-entropy-change alloys, fatigue-resistant composites, and polymer-based materials with improved thermal conductivity. Second, system-level optimization must address the fundamental trade-offs between performance metrics, requiring co-design of materials, actuators, and heat exchangers. Third, the exploration of niche applications where solid-state cooling offers unique advantages, such as electronics thermal management, specialized aerospace systems, or waste-heat-driven cooling, could provide pathways to commercialization before competing directly with large-scale vapor-compression systems. Finally, life-cycle assessment and recycling technologies for elastocaloric materials will be crucial for realizing the full sustainability potential of this technology.

As global demand for efficient, environmentally friendly cooling solutions continues to grow, elastocaloric cooling represents a viable path toward sustainable refrigeration. With continued interdisciplinary efforts in materials science, thermal engineering, and system mechanical design, this technology has the potential to evolve from laboratory prototypes to commercial systems that complement existing refrigeration technologies and contribute to global emission reduction goals. The coming years will likely see increased focus on standardizing performance metrics, improving operational stability, and demonstrating practical applications that highlight the unique advantages of solid-state caloric cooling.

Acknowledgements

This work was financially supported by the National Natural Science Foundation of China (Grant Nos. U2441272 and 52376015) and the HE Science Foundation.

References

[1] Eisenstein M 2025 *Nature* **637** 1008
[2] Baha M, Hammami S and Dupont J L 2025 *60th IIR Technical Brief on Refrigeration Technologies*, April, 2025, Paris, p. 13
[3] Mine O and Wilfried W 2024 *World Economic Forum*, June 25, 2024, p. 26
[4] Bonnot E, Romero R, Mañosa L, Vives E and Planes A 2008 *Phys. Rev. Lett.* **100** 125901
[5] Mevada H, Liu B, Gao L, Hwang Y, Takeuchi I and Radermacher R 2024 *Int. J. Refrig.* **162** 86
[6] Zhang F, Miao X, van Dijk N, Brück E and Ren Y 2024 *Adv. Energy Mater.* **14** 2400369
[7] Nehan P Z Z, Vitayaya O, Munazat D R, Manawan M T E, Darminto D and Kurniawan B 2024 *Phys. Chem. Chem. Phys.* **26** 14476
[8] Law J Y, Moreno-Ramírez L M, Díaz-García Á and Franco V *J Appl. Phys.* **133** 040903
[9] Du F, Yang T, Hao H, *et al.* 2025 *Nature* **640** 924
[10] Qian X, Han D, Zheng L, Chen J, Tyagi M, Li Q, Du F, Zheng S, Huang X, Zhang S, Shi J, Huang H, Shi X, Chen J, Qin H, Bernholc J, Chen X, Chen L Q, Hong L and Zhang Q M 2021 *Nature* **600** 664
[11] Han D, Zhang Y, Huang C, Zheng S, Wu D, Li Q, Du F, Duan H, Chen W, Shi J, Chen J, Liu G, Chen X and Qian X 2024 *Nature* **629** 1041
[12] Zheng S, Du F, Zheng L, Han D, Li Q, Shi J, Chen J, Shi X, Huang H, Luo Y, Yang Y, O'reilly P, Wei L, De Souza N, Liang H and Qian X 2023 *Science* **382** 1020
[13] Li Q, Wei L, Zhong N, Shi X, Han D, Zheng S, Du F, Shi J, Chen J, Huang H, Duan C and Qian X 2024 *Nat. Commun.* **15** 702
[14] Sun Y, An S, Gao Y, Yu Z, Yuan X, Ma Z, Shi K, Hu F and Wang C 2025 *J. Mater. Chem. A Mater.* **13** 6152
[15] Zhao X, Zhang Z, Hattori T, Wang J, Li L, Jia Y, Li W, Xue J, Fan X, Song R, Zhu J, Liu P, Chen X Q, Zhang Z and Li B 2025 *Nat. Commun.* **16** 7713
[16] Cirillo L, Greco A and Masselli C 2022 *Therm. Sci. Eng. Prog.* **33** 101380
[17] Xu J 2025 *Nat. Energy* **10** 1187
[18] IEA 2025 https://www.iea.org/reports/electricity-mid-year-update-2025 [accessed 5 January 2026]
[19] Mohamed M, Zakuan N D, Tengku Hassan T N A, Lock S S M and Mohd Shariff A 2024 *Sustainability* (Switzerland) 16 4089
[20] Su Y, Duan S, Kim J, Kim J K and Park J H 2025 *Metals and Materials International*
[21] Frenzel J, Wieczorek A, Opahle I, Maaß B, Drautz R and Eggeler G 2015 *Acta Mater.* **90** 213
[22] Mota-Babiloni A, Makhnatch P, Khodabandeh R and Navarro-Esbrí J 2017 *Int. J. Refrig.* **74** 680
[23] Karami M, Zhu Z, Chan K H, Hua P, Tamura N and Chen X 2024 *Phys. Rev. Lett.* **132** 066101
[24] Cui J, Wu Y, Muehlbauer J, Hwang Y, Radermacher R, Fackler S, Wuttig M and Takeuchi I 2012 *Appl. Phys. Lett.* **101** 073904
[25] Xiao F, Jin M, Liu J and Jin X 2015 *Acta Mater.* **96** 292
[26] Wu Y, Ertekin E and Sehitoglu H 2017 *Acta Mater.* **135** 158
[27] Li Q, Deng Z, Ahadi A, Chu K, Yan J, Huang K, Hu S, Ren Y, He B and Sun Q 2025 *Nat. Communs.* **16** 4511
[28] Cui J 2024 *Shape Mem. Superelast.* **10** 80
[29] Qian S, Wang Y, Geng Y, Wang Y, Ling J, Hwang Y, Radermacher R, Takeuchi I and Cui J 2016 *Int. J. Refrig.* **64** 1
[30] Bruederlin F, Ossmer H, Wendler F, Miyazaki S and Kohl M 2017 *J. Phys. D Appl. Phys.* **50** 424003
[31] Ersoy K 2025 *Eng. Proc.* **89** 42
[32] Cheng S 2023 *Phys. Scr.* **98** 075940
[33] Tušek J, Engelbrecht K and Pryds N 2016 *Sci. Technol. Built. Environ.* **22** 489
[34] Huang C, Liang J, Liu Z and Li T 2022 *Appl. Phys. Lett.* **121** 143901
[35] Zhou G, Li Z, Wang Q, Zhu Y, Hua P, Yao S and Sun Q 2024 *Nat. Energy* **9** 862
[36] Wang Y, Liu Y, Xu S, Zhou G, Yu J and Qian S 2023 *Comms. Eng.* **2** 79
[37] Xie Z, Sebald G and Guyomar D 2015 *Appl. Phys. Lett* **107** 081905
[38] Lünser K, Kavak E, Gürpinar K, Emre B, Atakol O, Stern-Taulats E, Porta M, Planes A, Lloveras P, Tamarit J L and Mañosa L 2024 *Nat. Commun.* **15** 6171
[39] Sebald G, Lombardi G, Coativy G, Jay J, Lebrun L and Komiya A 2023 *Appl. Therm. Eng.* **223** 120016
[40] Furst S J, Crews J H and Seelecke S 2012 *Continuum Mech. Therm.* **24** 485
[41] Otsuka K and Wayman C M 1998 *Shape Memory Materials* (Cambridge University Press) p. 37
[42] Boyd J G and Lagoudas D C 1996 *Int. J. Plast.* **12** 843
[43] Lagoudas D C, Bo Z and Qidwai M A 1996 *Mech. Compos. Mater. Struct.* **3** 153
[44] Lagoudas D C and Entchev P B 2004 *Mech. Mater.* **36** 865
[45] Suebsuk J, Horpibulsuk S and Liu M D 2010 *Comput. Geotech.* **37** 956

[46] Cui J, Chu Y S, Famodu O O, Furuya Y, Hattrick-Simpers J, James R D, Ludwig A, Thienhaus S, Wuttig M, Zhang Z and Takeuchi I 2006 *Nat. Mater.* **5** 286

[47] Muller I and Seelecke S 2001 *Math. Comput. Model* **34** 1307

[48] Furst S J, Crews J H and Seelecke S 2012 *Continuum Mech. Therm.* **24** 485

[49] Massad J E and Smith R C 2005 *Thin Solid Films* **489** 266

[50] Kim S J and Seelecke S 2007 *Int. J. Solids Struct.* **44** 1196

[51] Seelecke S, Kim S J, Ball B L and Smith R C 2005 *Continuum Mech. Therm.* **17** 337

[52] Wendler F, Ossmer H, Chluba C, Quandt E and Kohl M 2017 *Acta Mater.* **136** 105

[53] Schmidt M, Schütze A and Seelecke S 2015 *Int. J. Refrig.* **54** 88

[54] Li T, Alavy M and Siegel J A 2019 *Build Environ.* **150** 99

[55] Liang D, Wang Q, Chu K, Chen J, Hua P, Ren F and Sun Q 2022 *Appl. Mater. Today* **26** 101377

[56] Zhang J, Cheng S and Sun Q 2025 *Device* **3** 100677

[57] Lin H, Hua P, Li Y, Li Q, Yu K, Yan J, Onuki Y, Wang Q, Su C, Zhou G, Sato S, Huang K, Luan J, Lee Y K, Huang M, Yang Y, Ren Y and Sun Q 2026 *Mat. Sci. Eng. A* **949** 149449

[58] Hou H, Cui J, Qian S, Catalini D, Hwang Y, Radermacher R and Takeuchi I 2018 *MRS Bull* **43** 285

[59] Ahčin Ž and Tušek J 2023 *Appl. Therm. Eng.* **231** 120996

[60] Xie Z, Sebald G and Guyomar D 2016 *Appl. Phys. Lett.* **108** 041901

[61] Frenzel J, Eggeler G, Quandt E, Seelecke S and Kohl M 2018 *MRS Bull* **43** 280

[62] Kabirifar P, Žerovnik A, Ahčin Ž, Porenta L, Brojan M and Tušek J 2019 *Strojniski VestnikJournal Mech. Eng.* **65** 615

[63] Qian S, Wang Y, Geng Y, Ling J, Muehlbauer J, Hwang Y, Radermacher R and Takeuchi I 2016 16*th International Refrigeration and Air Conditioning Conference*, July 11, 2016, Purdue, p. 2385

[64] Qian S, Geng Y, Wang Y, Muehlbauer J, Ling J, Hwang Y, Radermacher R and Takeuchi I 2016 *Sci. Technol. Built. Environ.* **22** 500

[65] Ossmer H, Wendler F, Gueltig M, Lambrecht F, Miyazaki S and Kohl M 2016 *Smart Mater. Struct.* **25** 085037

[66] Engelbrecht K, Tušek J, Eriksen D, Lei T, Lee C Y, Tušek J and Pryds N 2017 *J Phys. D Appl. Phys.* **50** 424006

[67] Tušek J, Engelbrecht K, Eriksen D, Dall'Olio S, Tušek J and Pryds N 2016 *Nat. Energy* **1** 16134

[68] Chen Y, Wang Y, Sun W, Qian S and Liu J 2022 *A Compact Elastocaloric Refrigerator Innovation* **3** 16134

[69] Yao S, Dang P, Li Y, Wang Y, Zhang X, Liu Y, Qian S, Xue D and He Y L 2024 *Nat. Commun.* **15** 7203

[70] Zhou G, Zhang L, Li Z, Hua P, Sun Q and Yao S 2025 *Nature* **639** 87

[71] Masche M, Ianniciello L, Tušek J and Engelbrecht K 2021 *Int. J Refrig.* **121** 302

[72] Qian S 2023 *Appl. Therm. Eng.* **219** 119540

[73] Yang Y, Zhan J B, Sui J B, Li C Q, Yang K, Castany P and Gloriant T 2020 *Scr. Mater.* **188** 130

[74] Vanaei S, Mohajerani S, Rocco P, Sojoodi M, Pourshams M and Elahinia M 2025 *Shape Mem. Superelast.* **11** 115

[75] Wu Y, Liu Y and Qian S 2023 *Appl. Therm. Eng.* **221** 119819

[76] Emaikwu N, Catalini D, Muehlbauer J, Hwang Y, Takeuchi I and Radermacher R 2019 13*th International Conference on Energy Sustainability*, July 14–17, 2019, Bellevue, WA, USA

[77] Ianniciello L, Bartholomé K, Fitger A and Engelbrecht K 2022 *Appl. Therm. Eng.* **202** 117838

[78] Ahčin Ž, Dall'Olio S, Žerovnik A, Baškovič U Ž, Porenta L, Kabirifar P, Cerar J, Zupan S, Brojan M, Klemenc J and Tušek J 2022 *Joule* **6** 2338

[79] Qian S, Catalini D, Muehlbauer J, Liu B, Mevada H, Hou H, Hwang Y, Radermacher R and Takeuchi I 2023 *Science* **380** 722

[80] Mañosa L and Planes A 2024 *Shape Mem. Superelast.* **10** 89

[81] Xu J, Bruederlin F, Bumke L, Ossmer H, Quandt E, Miyazaki S and Kohl M 2024 *Shape Mem. Superelast.* **10** 1193

[82] Heremans J P 2016 *Tri-Technol. Device Refrig.* **9821** 98210

[83] Dang P, Zhang L, Zhou Y, Liang Q, Ding X, Sun J and Xue D 2023 *Scr. Mater.* **236** 115638

[84] Niitsu K, Kimura Y, Omori T and Kainuma R 2018 *NPG Asia Mater.* **10** 457

[85] Schmidt M, Ullrich J, Wieczorek A, Frenzel J, Eggeler G, Schütz A and Seelecke S 2016 *J. Vis. Exp.* **111** e53626

[86] Bruederlin F, Bumke L, Quandt E and Kohl M 2019 20*th International Conference on Solid State Sensors and Actuators*, June 23–27, 2019, Berlin, p. 1467

[87] Brüderlin F 2022 *Advanced Elastocaloric Cooling Devices Based on Shape Memory Alloy Films* (Ph. D. Dissertation) (Karlsruher Institut für Technologie)

[88] Bruederlin F, Bumke L, Chluba C, Ossmer H, Quandt E and Kohl M 2018 *Energy Technology* **6** 1588

[89] Sharar D J, Radice J, Warzoha R, Hanrahan B and Smith A 2021 *Appl. Phys. Lett.* **118** 184103

[90] Czernuszewicz A, Griffith L, Slaughter J and Pecharsky V 2020 *Appl. Mater. Today* **19** 100557

[91] Zhang J, Chen M, Luo W, Wei B, Luo T, Shen X, Li B and Zhu G 2025 *Nat. Sustain.* **8** 651

[92] Swoboda T, Klinar K, Yalamarthy A S, Kitanovski A and Muñoz Rojo M 2021 *Adv. Electron Mater* **7** 2000625

[93] Klinar K, Muñoz Rojo M, Kutnjak Z and Kitanovski A 2020 *J. Appl. Phys.* **127** 234101

[94] Baek K, Kim M, Kim H S, Ahn J and So H 2025 *Adv. Mater. Technol.* **10** e01848

[95] Kaur R, Tanwar A, O'Brien P and Razeeb K M 2025 *Appl. Therm. Eng.* **280** 128468

[96] Morhan M and Pittam G 2023 (PCT Patent) WO2023/242227 A2 [2023-12-21]

[97] Exergyn 2025 https://www.exergyn.com/technology/ [accessed 6 November 2025]

[98] Zhang J, Zhu Y, Cheng S, Yao S and Sun Q 2022 *Appl. Therm. Eng.* **213** 118657

[99] Zhou G, Zhu Y, Yao S and Sun Q 2023 *Joule* **7** 2003

[100] Porenta L, Trojer J, Brojan M and Tušek J 2022 *Int. J. Solids Struct* **256** 111948

[101] Dall'Olio S, Ahčin Ž, Žerovnik A, Kabirifar P, Brojan M and Tušek J 2024 *Shape Mem. Superelast.* **10** 99

[102] Ahčin Ž, Liang J, Engelbrecht K and Tušek J 2021 *Appl. Therm. Eng.* **190** 116842

[103] Qian S and Takeuchi I 2024 *Shape Memory and Superelasticity* **10** 162

[104] Li X, Cheng S and Sun Q 2022 *Appl. Therm. Eng.* **215** 118942

[105] Cheng S, Xiao Y, Li X, Lin H, Hua P and Sheng L 2023 *Int. J. Refrig.* **147** 39

[106] Li X, Hua P and Sun Q 2023 *Nat. Commun.* **14** 7982

[107] Li X, Hua P, Li Y, Hu J, Su C, Yao S and Sun Q 2025 *Cell Rep. Phys. Sci.* **6** 102669

[108] ISO. Non-ducted air conditioners and heat pumps - Testing and rating for performance: ISO 18326:2018[S/OL]. Geneva: International Organization for Standardization, 2018

[109] Standardization Administration of China. Minimum allowable values of energy efficiency and energy efficiency grades for room air conditioners: GB 21455-2019[S]. Beijing: Standards Press of China, 2019

[110] Mevada H, Hwang Y and Takeuchi I 2025 *Int. J. Refrig.* **180** 407

[111] Khosla R, Miranda N D, Trotter P A, Mazzone A, Renaldi R, McElroy C, Cohen F, Jani A, Perera-Salazar R and McCulloch M 2021 *Nat. Sustain* **4** 201

[112] Qian S, Wang Y, Yuan L and Yu J 2019 *Energy* **182** 881

[113] Qian S, Wang Y, Xu S, Chen Y, Yuan L and Yu J 2021 *Appl. Energy* **298**

[114] Yuan L, Wang Y, Yu J, Greco A, Masselli C and Qian S 2023 *Appl. Therm. Eng.* **218** 117269

[115] Zhu H, Li J, Lai C and Zhang H 2022 *Int. J. Hydrogen Energy* **47** 27124

[116] Han Y, Gao W and Qin Y 2025 *Appl. Therm. Eng.* **266** 125578

[117] Lu Z, Huang Y and Zhao Y 2023 *Renew Energy* **215** 118972

[118] Ma L, Zhao Q, Zhang H, Hou S, Zhao J, Wang F, Zhang C, Miao H and Yuan J 2022 *Energy* **239** 122290

[119] Qian S, Yao S, Wang Y, Yuan L and Yu J 2022 *Appl. Energy* **322** 119462

[120] Gao X, Yang J, Wu J, Xin X, Li Z, Yuan X, Shen X and Dong S 2020 *Adv. Mater. Technol.* **5** 1900716

[121] Ehl L, Scherer N, Zimmermann D, Trofimenko I, Molitor P, Kirsch S M, Louia F and Motzki P 2025 *Front. Mater.* **12** 1563997

[122] Bachmann N, Fitger A, Maier L M, Mahlke A, Schäfer-Welsen O, Koch T and Bartholomé K 2021 *Commun. Phys.* **4** 194

[123] Bachmann N, Schwarz D, Bach D, Schäfer-Welsen O, Koch T and Bartholomé K 2022 *Energies (Basel)* **15** 5089

[124] Wang R, Fang S, Xiao Y, *et al.* 2019 *Science* **366** 216

[125] Xiao Y, Mei G, Feng D, Zhao W, Guo W, Leng X, Qian D, Zhao W, Bai J, Wang Z, Zhu M, Zhou X and Liu Z 2024 *Adv. Mater.* **36** 2407009

[126] Zheng J, Li Z, Lv C, Li G, Huo X, Wang B, Zhang K, Bao R, Gan B, Zhao X and Hou H 2025 *J. Phys. D Appl. Phys.* **58** 075503

[127] Zhang Z, Guan Z, Wang Y, Hu J, Li Z, Yao J, Bao C, Zhang K and Li B 2025 *Materialia* **40** 102422

[128] Zhang S, Yang Q, Li C, Fu Y, Zhang H, Ye Z, Zhou X, Li Q, Wang T, Wang S, Zhang W, Xiong C and Wang Q 2022 *Nat. Commun.* **13** 9

[129] Zhang S, Fu Y, Nie X, Li C, Zhou Y, Wang Y, Yi J, Xia W, Song Y, Li Q, Xiong C, Qian S, Yang Q and Wang Q 2024 *Nat. Commun.* **15** 6567

[130] Sebald G, Lombardi G, Coativy G, Jay J, Lebrun L and Komiya A 2023 *Appl. Therm. Eng.* **223** 120016

[131] Greibich F, Schwödiauer R, Mao G, Wirthl D, Drack M, Baumgartner R, Kogler A, Stadlbauer J, Bauer S, Arnold N and Kaltenbrunner M 2021 *Nat. Energy* **6** 260

[132] Ludwig C and Kohl M 2024 *J. Appl. Phys.* **136** 165001

[133] Sion M, Jay J, Coativy G, Komiya A and Sebald G 2024 *J. Phys. Energy* **6** 025003

[134] Bianchi M, Fambri L, Fredi G, Pegoretti A and Dorigato A 2024 *Appl. Sci.* **14** 10525